RSC Advances

PAPER

View Article Online
View Journal | View Issue

Cite this: *RSC Adv.*, 2021, **11**, 4639

Singlet fission from upper excited singlet states and polaron formation in rubrene film†

Tong Wu,[a] Wenjun Ni,[a] Gagik G. Gurzadyan *[a] and Licheng Sun *[abc]

Femtosecond fluorescence up-conversion and transient absorption pump-probe setups are applied to study the relaxation dynamics of the lower and upper excited singlet electronic states in easy-to-make rubrene films. Upon 250 nm (4.96 eV) excitation, singlet fission was observed directly from S_2 state bypassing S_1 state within 30 fs *i.e.* breaking the classical Kasha rule. From the transient absorption measurements, polaron formation was also detected on the same time scale. Both singlet fission and polaron formation are accelerated from upper excited states compared with S_1 state. Our work shows that rubrene films with low degree of crystallinity could display efficient singlet fission, notably in the case of excitation to upper lying electronic states. This can strongly expand the applications of rubrene in organic electronics. Moreover, our results will provide a new direction for synthesizing novel materials with optimized excited state properties for organic photovoltaic applications.

Received 23rd December 2020
Accepted 14th January 2021

DOI: 10.1039/d0ra10780h

rsc.li/rsc-advances

1. Introduction

Singlet fission is a spin-allowed process in which a singlet excited state molecule shares its energy with an adjacent ground state molecule to generate two triplet excited state molecules.[1] Singlet fission has attracted a great deal of interest for its potential to increase photovoltaic efficiency above the Shockley–Queisser limit,[2,3] and has been observed in crystals,[4–6] films,[7,8] dimers,[9,10] nanoparticles[11,12] and concentrated solutions.[13] Singlet fission is very fast in solid tetracene and pentacene; triplet yield is reached 200%.[14–16] Rubrene as a derivative of tetracene, due to its high carrier mobility[17–19] and long exciton diffusion length,[20–22] has received extensive attention in recent years. Singlet fission has already been confirmed in rubrene crystal.[23–25] In our previous publications,[26,27] we studied rubrene crystal by femtosecond pump-probe spectroscopy; triplet states are formed within 2–20 ps *via* singlet fission from lowest excited singlet state under 500 nm excitation and within 200 fs from upper excited singlet states under 250 nm excitation. In ref. 28, by combining spectroscopic measurements and theoretical modeling, formation of correlated triplet pairs was confirmed in rubrene crystal within 20 fs. Miyata *et al.* reported that SF takes place through both the coherent and the incoherent pathways. Coherent phonons of singlet and triplet exciton states were observed in a rubrene single crystal at 35 K.[29,30] Apart from single crystal, triplet states are also studied in amorphous rubrene film, which originate from not only singlet fission but also polarons.[31] In ref. 32, it is reported that both singlet fission and triplet fusion (TF) can happen in amorphous rubrene; singlet fission undertakes a charge transfer state mediated channel and competes well with TF. In rubrene film, suppression of singlet fission at low temperatures was reported.[33–35] Earlier, it was also demonstrated in rubrene crystal.[27] Zhang's group reported the competition between singlet fission, fluorescence and dissociation in rubrene doped amorphous films.[36] They have also demonstrated that transition rate of singlet fission exponentially decreased with increasing distance between rubrene molecules.[37] Finton *et al.* presented the time-resolved fluorescence results of various film samples.[38] They have not observed quenching of fluorescence in fully amorphous samples, which indicates absence of singlet fission in this rubrene film. In the samples which contain some degree of crystallinity, fluorescence is strongly quenched, which is a sign for singlet fission.

It should be mentioned that the time-resolved spectroscopic data on dynamics of polaron and triplet formation are rather scarce and restricted to time-resolved fluorescence. Moreover, all pump-probe measurements involving upper excited singlet electronic states in rubrene film is still missing. In the present work, we draw the detailed picture of the relaxation pathways from the upper excited states in easy-to-make rubrene film. This may lead to advantageous applications in photovoltaics. Our approach is, by using molecular systems and crystals which have strong absorption in blue/UV, to produce triplet states *via* singlet fission directly from higher lying electronic states bypassing relaxed S_1 state. Thus it will necessarily lead to

[a]*State Key Laboratory of Fine Chemicals, Institute of Artificial Photosynthesis, Dalian University of Technology, 116024 Dalian, China. E-mail: gurzadyan@dlut.edu.cn; lichengs@kth.se*

[b]*Department of Chemistry, School of Engineering Sciences in Chemistry, Biotechnology and Health, KTH Royal Institute of Technology, 10044 Stockholm, Sweden*

[c]*Center of Artificial Photosynthesis for Solar Fuels, School of Science, Westlake University, 310024, Hangzhou, China*

† Electronic supplementary information (ESI) available. See DOI: 10.1039/d0ra10780h

increase of efficiency of photon-to-electron conversion. Harnessing the entire UV/blue/Vis spectrum of the Sun for producing free charge careers *via* singlet fission may have far-reaching advantages and enormous industrial benefits.

There are few possible detection methods: magnetic field effect to recognize SF qualitatively;[39,40] time-resolved fluorescence to identify the quenching of singlet state,[41,42] time-resolved resonance Raman and time-resolved two-photon photoemission spectroscopy to distinguish various intermediate states,[43–46] 2D, 3D spectroscopy[47,48] and ultrafast pump-probe method to track the decay of singlet state and the formation of triplet state and, possibly, also identifying intermediate states.

In this work, we used time-resolved fluorescence and pump-probe transient absorption techniques with time resolution of 30 fs, in order to study various photoreactions after excitation of upper excited electronic states of rubrene film, *i.e.* singlet exciton fission, triplet–triplet annihilation, polaron formation (Scheme 1).

2. Materials and methods

2.1 Sample preparation

Rubrene was thermally evaporated in Vacuum Evaporation Pump device with a pressure below 10^{-4} Pa [QHV-Z350C, Pana Instruments]. Before installing in the chamber, the quartz substrates were cleaned by ethanol in ultrasonic bath for 10 minutes and stood in ethanol for 12 hours. After that, the quartz substrates were treated with plasma in an O_3-filled environment for 8 minutes in order to remove organic impurities and contaminants. X-ray diffraction (XRD) measurements were performed to characterize crystal structure of our films, using data acquisition mode 1D. Besides, the surface of our films was investigated by use of scanning electron microscopy (SEM) and atomic force microscopy (AFM). SEM images were measured under 5 kV accelerating voltage and 10 A current. AFM was conducted on Tecnai F30 operated at 300 kV, in non-contact mode with the scan rate of 1.0 Hz.

2.2 Experimental

The steady state absorption spectra were obtained by using UV-Visible spectrophotometer (Cary 100, Agilent) and fluorescence spectra are recorded by spectrofluorometer (Flurorolog-3, HORIBA Jobin Yvon). In both cases the wavelength resolution was 1 nm.

Time-resolved up-conversion measurements were carried out by a fluorescence spectrometer (TRFLS, Newport) with 100 fs resolution in combination with a mode-locked Ti-sapphire laser (Mai Tai DeepSee, Spectra-Physics). Briefly, the femtosecond laser system generated light pulses at 800 nm of duration 150 fs at a repetition rate 80 MHz, average power of 2.9 W. The frequency of the laser pulse was doubled with a BBO crystal and served for excitation (pump), gate pulse was split from the pump beam with beam splitter. The emitted fluorescence was focused into a BBO crystal together with the gate beam (800 nm) to create the up-converted signal at the sum-frequency generation (SFG). The fluorescence decay curve is obtained by varying the optical path of the delay stage for the gate beam. Fluorescence lifetimes in the range 10 ps to 100 ns were measured by time-correlated single photon counting (TCSPC) technique (PicoHarp 300, PicoQuant). By use of deconvolution/fit program (FluFit, PicoQuant) the time resolution was reached down to 10 ps. The second harmonic of a Titanium–sapphire laser (Mai Thai DeepSee, Spectra-Physics) at 400 nm (150 fs, 80 MHz) was used as the excitation source.

The transient absorption (TA) spectra were measured by optical femtosecond pump-probe spectroscopy. The output of a mode-locked Ti-sapphire amplified laser system (Spitfire Ace, Spectra-Physics) with wavelength 800 nm, pulse-width 35 fs, repetition rate 1 kHz, average power 4 W was split into two beams (10 : 1). Pump beam in the range of 240–2400 nm is acquired by use of Optical Parametric Amplifier (TOPAS, Light Conversion). 10% of 800 nm laser pulse was focused in a 3 mm thickness rotated CaF_2 plate to produce a white light continuum (WLC), which was used as a probe beam ranging between 350 and 850 nm. Home-built pump-probe setup was used for obtaining transient absorption spectra and kinetics. The relative polarizations between pump and probe beam were arranged to the magic angle (54.7°) to avoid rotational depolarization effects (except for $\lambda_{pump} = 250$ nm). The experimental data were fitted to a multiexponential decay function convoluted with the instrument response function $B(t - t_0)$ centered at t_0:

$$\Delta A(t) = \int_0^\infty \left(\Delta A_0 + \sum_{i=1}^{n} \Delta A_i \exp\left(-\frac{t'}{t_i}\right) \right) B(t - t' - t_0) \mathrm{d}t'$$

Here $\Delta A(t)$ is the difference absorption at time t, ΔA_i is the amplitude of the component with lifetime τ_i and ΔA_0 is the offset due to long-living species. The instrument response function was modeled by a Gaussian with a variable Full Width Half Maximum (FWHM). Deconvolution fit process allows obtaining three times higher resolution than the pulse width of the laser, *i.e.* 20–30 fs.[49–51]

Global fit of time-resolved experimental results was done by Glotaran software.[52] The decay associated spectra (DAS) allow separating several overlapping emission spectra in parallel model, whereas the evolution associated spectra (EAS) shows the global fit results in a sequential model.

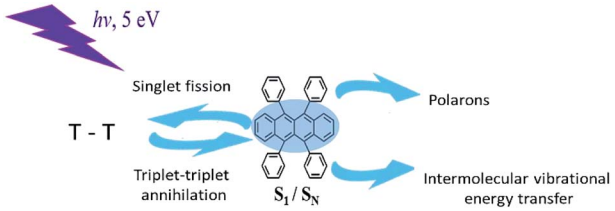

Scheme 1 Various photophysical processes in rubrene.

3. Results and discussion

3.1 Characterization of rubrene film

Our film was fully characterized by use of XRD, SEM and AFM techniques (Fig. S1†). In the XRD spectrum (Fig. S1a†), there

exists a peak at 27° repeating the reference rubrene crystal, similar to previous observations.[53] It is indicative of certain amount of crystallinity of orthorhombic form in our films. Besides, the SEM image exhibits clear polycrystalline morphology of 10–20 micrometer size. The AFM picture (inset of Fig. S1b†) gives a proof of smooth and uniform film surface. Note that the beam size during pump-probe and time-resolved fluorescence is about 100 μm, *i.e.* fully covering both amorphous and crystalline regions.

3.2 Steady state and time-resolved PL characterizations

Steady-state absorption, fluorescence and excitation spectra of rubrene in hexane and film are presented in Fig. 1a and b, respectively. We use absorptance ($1 - T$, where T is transmittance) as a linear scale of absorption instead of absorbance. Absorption spectrum of rubrene solution shows four maxima at 522, 487, 457 and 431 nm, ascribed to the $S_0 \rightarrow S_1$ band[54] with a vibronic progression of $\Delta\omega = 1300\ cm^{-1}$, which corresponds well to literature data.[26] The fluorescence spectrum exhibits two maxima, at 551 and 589 nm, with vibronic progression $\Delta\omega = 1170\ cm^{-1}$. Absorption and excitation spectra match well, in agreement with Kasha rule.

Absorption spectrum of rubrene film also shows four maxima, at 528, 494, 464 and 434 nm with vibronic progression $\Delta\omega = 1300\ cm^{-1}$, which are red shifted by 7 nm compared with solution. The fluorescence spectrum shows two maxima, at 566 and 604 nm, indicative of a vibronic progression with $\Delta\omega = 1110\ cm^{-1}$; it is also red shifted relative to solution (15 nm), which is due to excitonic states originated from intermolecular interactions[54,55] and reabsorption.[54] The other reason for red shift is higher polarizability and the broadening of spectra as a result of static disorder.[33]

TCSPC map of rubrene solution at $\lambda_{ex} = 400$ nm (Fig. S2a†) corresponds well with the steady state fluorescence spectrum. The kinetics at different emission wavelengths (Fig. S2b†) shows mono-exponential decay with $\tau = 10$ ns.

Fig. 2 presents the TCSPC measurements of rubrene film under 400 nm excitation. We have observed a strong fluorescence quenching which indicates presence of a new non-radiative relaxation channel. Lifetimes are emission wavelength dependent and kinetics at all probe wavelengths are well fitted by 3 components (Table S1†): $\tau_1 = 68$–380 ps ($A_1 = 0.78$–0.21), $\tau_2 = 580$–1400 ps ($A_2 = 0.17$–0.49) and $\tau_3 = 3700$–5000 ps ($A_3 = 0.04$–0.30). The initial decay τ_1, which we assign to prompt fluorescence, is followed by a long component τ_3. This decay feature is typical for singlet fission followed by triplet–triplet annihilation (TTA), which has previously been observed in rubrene[27] and tetracene crystals.[14] We therefore suggest that in our case as well the observed delayed fluorescence is a result of singlet fission and further TTA. τ_2 most probably originates from oxidized rubrene.[26,56,57] Other reason can be existence of rubrene molecules with poor packing geometry where SF does not occur efficiently.

In order to obtain precise fluorescence lifetimes, the up-conversion measurements with 100 fs resolution were performed. Up-conversion fluorescence with higher time resolution (Fig. S3†) leads to an additional shorter time component of $\tau_1 = 1.4$–9.6 ps (Table S1†), which is due to direct fission from higher vibrational states and $\tau_2 = 30$–300 ps corresponds to the thermally activated singlet fission.[27]

From transient fluorescence results, we identify that singlet fission takes place in rubrene film. Further proof was obtained by combining the fluorescence data with the transient absorption measurements described below.

3.3 Femtosecond transient absorption spectra

In order to make proper assignments of the TA spectral bands, the pump-probe measurements were first performed in solution. Femtosecond transient absorption spectra under different excitation wavelengths are shown in Fig. 3. At $\lambda_{ex} = 480$ nm, a strong ESA at 430 nm appears promptly after photoexcitation and decays within 8.0 ns (Fig. 3b), is due to singlet–singlet absorption ($S_1 \rightarrow S_N$).[26] The negative part at 520–550 nm, which corresponds to maximum of steady state absorption, is due to ground state bleaching (GSB). The amplitude of GSB is small, similar to rubrene crystal[26,28] and film.[31] There are several reasons for the absence of GSB. One reason is an unfavorable orientation of the $S_0 \rightarrow S_1$ transition dipole in crystal.[28] Other reason is that the photoinduced absorption band between 2.4 and 2.6 eV overlaps substantially with the GSB in film.[31] The

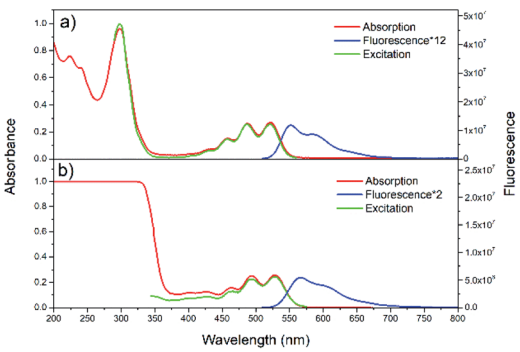

Fig. 1 Steady-state absorption, fluorescence, and excitation spectra of rubrene in hexane (a) ($\lambda_{ex} = 500$ nm, $\lambda_{em} = 570$ nm) and film (b) ($\lambda_{ex} = 480$ nm, $\lambda_{em} = 600$ nm).

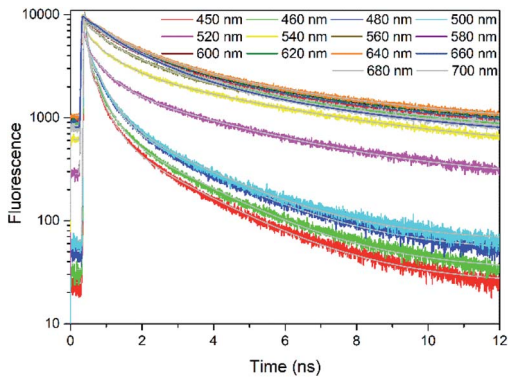

Fig. 2 TCSPC kinetics of rubrene film at different probe wavelengths, $\lambda_{ex} = 400$ nm. Pump fluence: 3.49×10^{-8} J cm^{-2}.

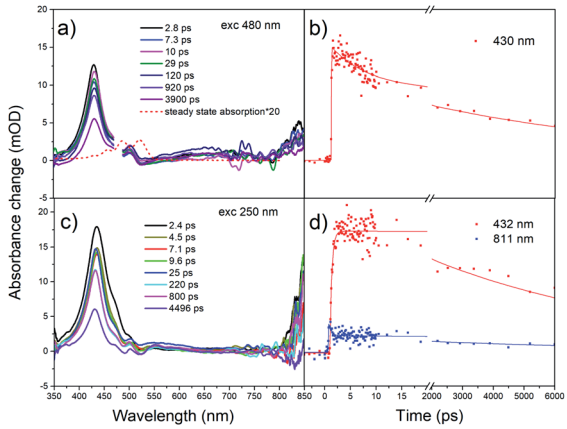

Fig. 3 Femtosecond transient absorption spectra for rubrene in hexane at (a) $\lambda_{ex} = 480$ nm, pump fluence: 7.60×10^{-4} J cm^{-2} and (c) $\lambda_{ex} = 250$ nm, pump fluence: 1.27×10^{-3} J cm^{-2}. (b and d) Transient kinetics at different wavelengths.

third reason is that the excited state absorption is much stronger than the GSB,[26] *i.e.* the molar extinction coefficient of the singlet–singlet absorption $S_1 \rightarrow S_N$ is significantly larger than that of $S_0 \rightarrow S_1$, $\varepsilon = 9550$–$12\,000$ M^{-1} cm^{-1}.[58,59] Because of small quantum yield of intersystem crossing ($\Phi < 0.01$),[60] we did not observe formation of triplet states (no triplet–triplet absorption TA band at about 500 nm).

Further, we have excited rubrene in hexane with $\lambda_{ex} =$ 250 nm, thus populating higher vibrational levels of S_2 state; transient absorption spectra are shown in Fig. 3c. The peak at 432 nm, *i.e.* ESA due to $S_1 \rightarrow S_N$ transition, decays within 7.5 ns (S_1 lifetime). The kinetics (Fig. 3d) shows a rise time of 0.39 ps, which is due to $S_2 \rightarrow S_1$ internal conversion. Relatively long S_2 lifetime is due to large S_1–S_2 energy gap (~2 eV), which is supported by DFT and TD-DFT calculations (ESI, Pages S8–S13†). Strong ESA band at 800–850 nm appears promptly after excitation; it is assigned to radical cation and anion.[61,62] These radicals form only at 250 nm (4.96 eV) excitation, and not at 480 nm (2.58 eV) or 340 nm (3.65 eV) which is indicative of an energy threshold for their formation. The ionization energy threshold is 6.4 eV in gas,[63] 4.95 eV for rubrene crystal and 5.3 eV for amorphous film.[64] The lifetime of the cation/anion is 0.50 ps (Fig. 3d). Similar results were obtained after excitation of the lower vibrational levels of S_2 ($\lambda_{ex} = 340$ nm, Fig. S4†).

Global fit of spectra under $\lambda_{ex} = 250$ nm (Fig. S5†) results in two time components: $\tau_1 = 0.90$ ps with maximum at 445 nm and $\tau_2 = 7.9$ ns with maximum at 433 nm. Time component of 7.9 ns corresponds to $S_1 \rightarrow S_N$ absorption, in agreement with fluorescence lifetime. The short component, 0.9 ps, is assigned to $S_2 \rightarrow S_M$ transition; decay of S_2 state is accompanied with the rise of S_1 population with the same time component.

The pump-probe measurements were carried out in rubrene film under different excitation wavelengths. For transient absorption spectra under $\lambda_{ex} = 480$ nm (Fig. S6†), we only observed one positive band at 439 nm. Similar to rubrene solution, we assign 439 nm band to singlet–singlet absorption. We do not observe triplet transient, indicating the absence of singlet fission. However, in rubrene crystal, singlet fission proceeds at even longer excitation wavelengths, *e.g.* $\lambda_{ex} =$ 500 nm.[26] The explanation is that in film, although molecules packed tightly, short-range molecular order matching the molecular arrangement in orthorhombic rubrene crystals is not favoured. Overall films are of low degree of crystallinity. Therefore, in rubrene film singlet fission undergoes under higher excitation photon energies 3–5 eV (400–250 nm, see below).

Under 400 nm excitation, the transient absorption spectra (Fig. 4a) present one small peak at 439 nm and another strong one at 489 nm. The 439 nm peak is assigned to singlet–singlet absorption, *i.e.* at the same position as with $\lambda_{ex} = 480$ nm. The band at 489 nm has a long decay time (over 100 ns, $A = 0.41$). We assign it to triplet absorption according to previous publications on the rubrene solution, film and crystal: 472 and 505 nm in solution,[65] 504 nm in film,[31] 510 nm in crystal.[24,26,27] Existence of decay times 29 ps ($A = 0.34$) and 2.4 ns ($A = 0.25$) in triplet ESA kinetics is due to overlap with singlet–singlet absorption band (439 nm). We suggest that triplet formation is due to singlet fission.

Similar results were obtained under 340 nm excitation (Fig. S7†). However, there is only triplet–triplet absorption peak locating at 490 nm, which is the result of singlet fission. The singlet–singlet TA band is much weaker and therefore is fully covered by strong triplet TA band. Moreover, both bands are strongly overlapping with polaron band (see below), overall causing some distortion.

The transient absorption spectra of rubrene film under 250 nm excitation are presented in Fig. 5a. At 441 nm (singlet–

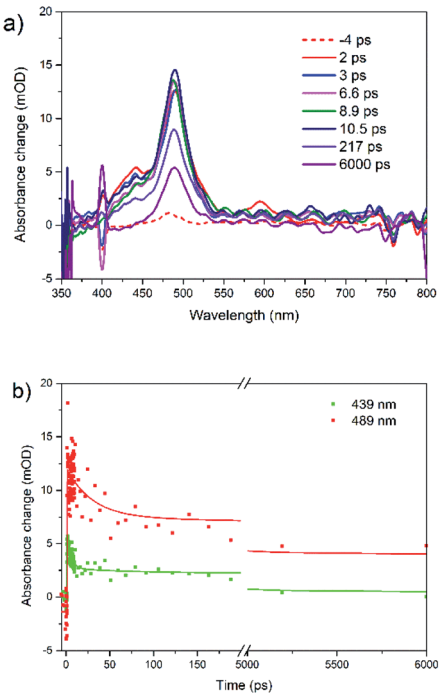

Fig. 4 (a) Femtosecond transient absorption spectra for rubrene film at $\lambda_{ex} = 400$ nm and (b) transient kinetics at 439 and 489 nm, pump fluence: 1.27×10^{-3} J cm^{-2}.

singlet absorption), we observed an ultrashort decay time of 0.26 ps (Table S2†). The shortening is due to direct singlet fission from S_2 state, *i.e.* $S_2 \rightarrow 2T_1$, which agrees well with 0.2 ps fission from S_N states in rubrene crystal.[26] No risetime was observed for the triplet transient, *i.e.* singlet fission proceeds within 30 fs (time resolution of our setup). Singlet fission competes well with ultrafast internal conversion $S_2 \rightarrow S_1$. As was indicated above, this is due to relatively long S_2 lifetime as a result of large S_1–S_2 energy gap: (~2 eV). We can also rule out participation of upper triplet states in population of T_1 *via* intersystem crossing $S_N \rightarrow T_N$ and further internal conversion $T_N \rightarrow T_1$ because T_N ($n = 2$) lifetimes of organic molecules are in pico- or nanosecond time scale [ref. 66 and references therein]. Polarons are observed at 706 nm which appears immediately after excitation, *i.e.* they are generated within instrument resolution 30 fs. Compared with 0.11 ps upon 340 nm excitation, polaron formation is faster under higher excitation photon energy. The ultrafast formation of polarons has also been observed in other molecules, *e.g.* the relaxation time of free exciton to form an exciton polaron is determined as 50 ± 23 fs in MEH-PPV[67] and 60–100 fs in the polymer PHTDMABQ.[68]

In film, we did not observe isosbestic point in the 400–550 nm region as in rubrene crystal,[26] which is indicative of more than one process contributing to the transient absorption. Here, under 250 nm excitation, the ESA band is broader, which indicates polarons absorb at 400–550 nm, *i.e.* strongly overlapping with triplet states. The decay times 220 ps (λ_{ex} = 340 nm) and 140 ps (λ_{ex} = 250 nm) at 490 nm are assigned to polarons lifetime, which recombine due to a secondary recombination processes *via* diffusion.[69] At "minus delays" (*i.e.* delay times of 1 ms) we observed TA signal in the range of 400–550 nm (Fig. S8†), indicating the polarons lifetime is longer than 1 ms. In our case, polarons absorb in the whole range of 400–800 nm. Singlet fission competes with polaron generation in our films with certain degree of crystallinity. Note that polarons are also formed in fully amorphous films.[70–72]

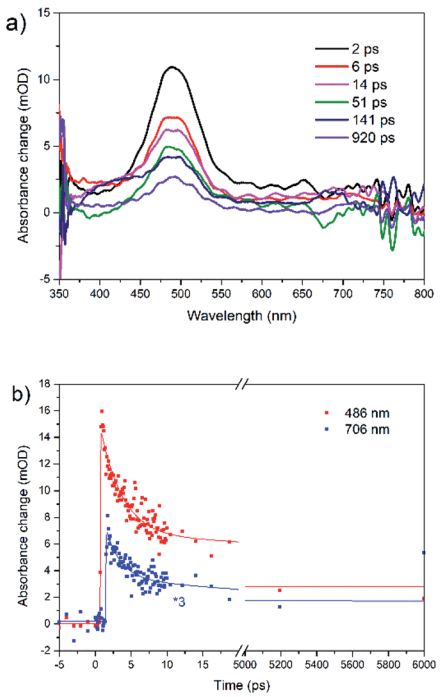

Fig. 5 (a) Femtosecond transient absorption spectra for rubrene film at λ_{ex} = 250 nm, pump fluence: 1.27 × 10^{-3} J cm^{-2}. (b) Transient kinetics at different wavelengths.

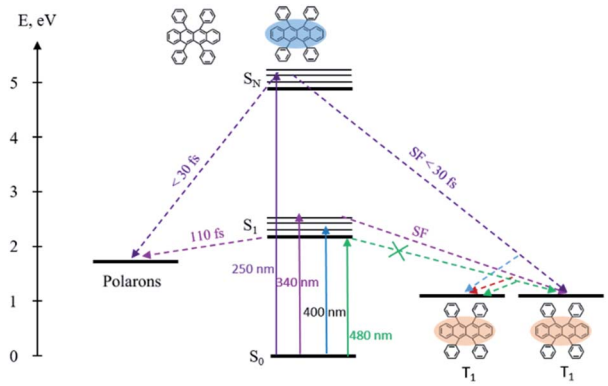

Scheme 2 Energy levels, excitation and relaxation in the rubrene film.

Our sample contains both amorphous and polycrystalline morphology. The beam size during pump-probe and time-resolved fluorescence is about 100 μm, which can fully cover both amorphous and crystalline regions. Considering all above, we conclude that rubrene films with low degree of crystallinity could display efficient singlet fission, which can strongly expand the applications of rubrene in organic electronics.

The overall relaxation processes after excitation with various photon energies are presented in Scheme 2. Population of the lowest singlet state results in the generation of polarons, moreover singlet fission is fully suppressed. Excitation of upper electronic states leads to 3 times faster polaron formation and to ultrafast singlet fission.

4. Conclusions

We have studied the excited state dynamics of easy-to-make rubrene film by femtosecond pump-probe and fluorescence spectroscopy under various excitation conditions. Upon excitation at 250 nm, an ultrafast (30 fs) singlet fission directly from higher excited singlet states was observed. Moreover, an ultrafast polaron formation was also detected at this excitation conditions. Both SF and polaron formation are accelerated after excitation of upper states compared with S_1 excitation. TD-DFT calculations support our observations.

Our film which contains both amorphous and polycrystalline morphology could display efficient singlet fission. The present results highlight potential of simple-fabricated and commercially attractive rubrene film in organic photovoltaic applications. Moreover, our work gives new insight into the dynamics of excited states in rubrene film, which will contribute in understanding of singlet fission in various organic crystals and films.

Author contributions

T. W. prepared and characterised the film, T. W., W. N. and G. G. G. performed all spectroscopic measurements and analysis, G. G. G. and L. S. supervised the research. All authors contributed in discussion and writing the manuscript.

Conflicts of interest

There are no conflicts to declare.

Acknowledgements

We are indebted to Prof. Maxim Gelin (Hangzhou Dianzi University) for valuable comments and suggestions. This work was supported by DUT startup grant and by DUT basic research funding (DUT18GJ205).

Notes and references

1 M. B. Smith and J. Michl, *Chem. Rev.*, 2010, **110**, 6891–6936.
2 M. B. Smith and J. Michl, *Rev. Phys. Chem.*, 2013, **64**, 361–386.
3 D. N. Congreve, J. Lee, N. J. Thompson, E. Hontz, S. R. Yost, P. D. Reusswig, M. E. Bahlke, S. Reineke, T. Van Voorhis and M. A. Baldo, *Science*, 2013, **340**, 334–337.
4 K. Aryanpour, A. Shukla and S. Mazumdar, *J. Phys. Chem. C*, 2015, **119**, 6966–6979.
5 R. J. Dillon, G. B. Piland and C. J. Bardeen, *J. Am. Chem. Soc.*, 2013, **135**, 17278–17281.
6 N. Renaud and F. C. Grozema, *J. Phys. Chem. Lett.*, 2015, **6**, 360–365.
7 S. T. Roberts, R. E. McAnally, J. N. Mastron, D. H. Webber, M. T. Whited, R. L. Brutchey, M. E. Thompson and S. E. Bradforth, *J. Am. Chem. Soc.*, 2012, **134**, 6388–6400.
8 J. N. Schrauben, J. L. Ryerson, J. Michl and J. C. Johnson, *J. Am. Chem. Soc.*, 2014, **136**, 7363–7373.
9 E. G. Fuemmeler, S. N. Sanders, A. B. Pun, E. Kumarasamy, T. Zeng, K. Miyata, M. L. Steigerwald, X. Y. Zhu, M. Y. Sfeir, L. M. Campos and N. Ananth, *ACS Cent. Sci.*, 2016, **2**, 316–324.
10 W. Ni, G. G. Gurzadyan, J. Zhao, Y. Che, X. Li and L. Sun, *J. Phys. Chem. Lett.*, 2019, **10**, 2428–2433.
11 R. D. Pensack, A. J. Tilley, S. R. Parkin, T. S. Lee, M. M. Payne, D. Gao, A. A. Jahnke, D. G. Oblinsky, P. Li, J. E. Anthony, D. S. Seferos and G. D. Scholes, *J. Am. Chem. Soc.*, 2015, **137**, 6790–6803.
12 M. J. Y. Tayebjee, K. N. Schwarz, R. W. MacQueen, M. Dvořák, A. W. C. Lam, K. P. Ghiggino, D. R. McCamey, T. W. Schmidt and G. J. Conibeer, *J. Phys. Chem. C*, 2016, **120**, 157–165.
13 B. J. Walker, A. J. Musser, D. Beljonne and R. H. Friend, *Nat. Chem.*, 2013, **5**, 1019–1024.
14 J. J. Burdett, A. M. Müller, D. Gosztola and C. J. Bardeen, *J. Chem. Phys.*, 2010, **133**, 144506.
15 C. Jundt, G. Klein, B. Sipp, J. Le Moigne, M. Joucla and A. A. Villaeys, *Chem. Phys. Lett.*, 1995, **241**, 84–88.
16 A. Rao, M. W. B. Wilson, J. M. Hodgkiss, S. Albert-Seifried, H. Bässler and R. H. Friend, *J. Am. Chem. Soc.*, 2010, **132**, 12698–12703.
17 V. Podzorov, E. Menard, A. Borissov, V. Kiryukhin, J. A. Rogers and M. E. Gershenson, *Phys. Rev. Lett.*, 2004, **93**, 86602.
18 V. C. Sundar, *Science*, 2004, **303**, 1644–1646.
19 T. Hasegawa and J. Takeya, *Adv. Mater.*, 2009, **10**, 024314.
20 P. Irkhin and I. Biaggio, *Phys. Rev. Lett.*, 2011, **107**, 17402.
21 J. C. Johnson, A. J. Nozik and J. Michl, *J. Am. Chem. Soc.*, 2010, **132**, 16302–16303.
22 H. Najafov, B. Lee, Q. Zhou, L. C. Feldman and V. Podzorov, *Nat. Mater.*, 2010, **9**, 938–943.
23 K. Bera, C. J. Douglas and R. R. Frontiera, *J. Phys. Chem. Lett.*, 2017, **8**, 5929–5934.
24 L. Ma, G. Galstyan, K. Zhang, C. Kloc, H. Sun, C. Soci, M. E. Michel-Beyerle and G. G. Gurzadyan, *J. Chem. Phys.*, 2013, **138**, 184508.
25 A. Ryasnyanskiy and I. Biaggio, *Phys. Rev. B: Condens. Matter Mater. Phys.*, 2011, **84**, 193203.
26 L. Ma, K. Zhang, C. Kloc, H. Sun, M. E. Michel-Beyerle and G. G. Gurzadyan, *Phys. Chem. Chem. Phys.*, 2012, **14**, 8307–8312.
27 L. Ma, K. Zhang, C. Kloc, H. Sun, C. Soci, M. E. Michel-Beyerle and G. G. Gurzadyan, *Phys. Rev. B: Condens. Matter Mater. Phys.*, 2013, **87**, 201203.
28 I. Breen, R. Tempelaar, L. A. Bizimana, B. Kloss, D. R. Reichman and D. B. Turner, *J. Am. Chem. Soc.*, 2017, **139**, 11745–11751.
29 K. Miyata, Y. Kurashige, K. Watanabe, T. Sugimoto, S. Takahashi, S. Tanaka, J. Takeya, T. Yanai and Y. Matsumoto, *Nat. Chem.*, 2017, **9**, 983–989.
30 K. Miyata, S. Tanaka, T. Sugimoto, K. Watanabe, T. Uemura, J. Takeya and Y. Matsumoto, *et al.*, *Ultrafast Phenomena XIX*, ed. K. Yamanouchi, Spring-Verlag, Berlin, 2015, pp. 218–221.
31 V. Jankus, E. W. Snedden, D. W. Bright, E. Arac, D. Dai and A. P. Monkman, *Phys. Rev. B: Condens. Matter Mater. Phys.*, 2013, **87**, 224202.
32 P. Sher, C. Chen, T. Chiu, C. Lin, J. Wang and J. Lee, *J. Phys. Chem. C*, 2019, **123**, 3279–3284.
33 G. B. Piland, J. J. Burdett, D. Kurunthu and C. J. Bardeen, *J. Phys. Chem. C*, 2013, **117**, 1224–1236.
34 J. Li, Z. Chen, Q. Zhang, Z. Xiong and Y. Zhang, *Org. Electron.*, 2015, **26**, 213–217.
35 Y. Zhang, Y. Lei, Q. Zhang and Z. Xiong, *Org. Electron.*, 2014, **15**, 577–581.
36 J. Li, Z. Chen, Y. Lei, Z. Xiong and Y. Zhang, *Synth. Met.*, 2015, **207**, 13–17.
37 X. Tian, L. Zhou, X. Chen, Y. Meng, Z. Xiong, X. Zhou and Y. Zhang, *Org. Electron.*, 2017, **50**, 429–434.
38 D. M. Finton, E. A. Wolf, V. S. Zoutenbier, K. A. Ward and I. Biaggio, *AIP Adv.*, 2019, **9**, 95027.
39 S. Kawata, Y. Pu, A. Saito, Y. Kurashige, T. Beppu, H. Katagiri, M. Hada and J. Kido, *Adv. Mater.*, 2016, **28**, 1585–1590.
40 T. Yago, K. Ishikawa, R. Katoh and M. Wakasa, *J. Phys. Chem. C*, 2016, **120**, 27858–27870.

41 B. Manna, A. Nandi and R. Ghosh, *J. Phys. Chem. C*, 2018, **122**, 21047–21055.
42 G. B. Piland and C. J. Bardeen, *J. Phys. Chem. Lett.*, 2015, **6**, 1841–1846.
43 A. J. Musser, M. Maiuri, D. Brida, G. Cerullo, R. H. Friend and J. Clark, *J. Am. Chem. Soc.*, 2015, **137**, 5130–5139.
44 C. Wang and M. J. Tauber, *J. Am. Chem. Soc.*, 2010, **132**, 13988–13991.
45 W. L. Chan, M. Ligges, A. Jailaubekov, L. Kaake, L. Miaja-Avila and X. Y. Zhu, *Science*, 2011, **334**, 1541–1545.
46 W. Chan, M. Ligges and X. Zhu, *Nat. Chem.*, 2012, **4**, 840–845.
47 A. C. Jones, N. M. Kearns, J. Ho, J. T. Flach and M. T. Zanni, *Nat. Chem.*, 2020, **12**, 40–47.
48 A. Mandal, M. Chen, E. D. Foszcz, J. D. Schultz, N. M. Kearns, R. M. Young, M. T. Zanni and M. R. Wasielewski, *J. Am. Chem. Soc.*, 2018, **140**, 17907–17914.
49 J. Shang, S. Yan, C. Cong, H. Tan, T. Yu and G. G. Gurzadyan, *Opt. Mater. Express*, 2012, **2**, 1713.
50 J. Shang, T. Yu, J. Lin and G. G. Gurzadyan, *ACS Nano*, 2011, **5**, 3278–3283.
51 S. Ullrich, T. Schultz, M. Z. Zgierski and A. Stolow, *Phys. Chem. Chem. Phys.*, 2004, **6**, 2796.
52 J. J. Snellenburg, S. P. Laptenok, R. Seger, K. M. Mullen and I. H. M. Stokkum, *J. Stat. Softw.*, 2012, **49**, 1–22.
53 K. Lin, Y. Wang, K. Chen, C. Ho, C. Yang, J. Shen and K. Chiu, *Sci. Rep.*, 2017, **7**, 40824.
54 P. Irkhin, A. Ryasnyanskiy, M. Koehler and I. Biaggio, *Phys. Rev. B: Condens. Matter Mater. Phys.*, 2012, **86**, 085143.
55 X. Zeng, D. Zhang, L. Duan, L. Wang, G. Dong and Y. Qiu, *Appl. Surf. Sci.*, 2007, **253**, 6047–6051.
56 C. Kloc, K. J. Tan, M. L. Toh, K. K. Zhang and Y. P. Xu, *Appl. Phys. A*, 2009, **95**, 219–224.
57 O. Mitrofanov, D. V. Lang, C. Kloc, J. M. Wikberg, T. Siegrist, W. Y. So, M. A. Sergent and A. P. Ramirez, *Phys. Rev. Lett.*, 2006, **97**, 166601.
58 C. Burgdorff, S. Ehrhardt and H. G. Loehmannsroeben, *J. Phys. Chem.*, 1991, **95**, 4246–4249.
59 T. Petrenko, O. Krylova, F. Neese and M. Sokolowski, *New J. Phys.*, 2009, **11**, 15001.
60 S. J. Strickler and R. A. Berg, *J. Chem. Phys.*, 1962, **37**, 814–822.
61 A. Saeki, S. Seki, T. Takenobu, Y. Iwasa and S. Tagawa, *Adv. Mater.*, 2008, **20**, 920–923.
62 S. Tao, H. Matsuzaki, H. Uemura, H. Yada, T. Uemura, J. Takeya, T. Hasegawa and H. Okamoto, *Phys. Rev. B: Condens. Matter Mater. Phys.*, 2011, **83**, 075204.
63 N. Sato, K. Seki and H. Inokuchi, *J. Chem. Soc., Faraday Trans. 2*, 1981, **77**, 1621.
64 Y. Nakayama, S. Machida, T. Minari, K. Tsukagishi, Y. Noguchi and H. Ishii, *Appl. Phys. Lett.*, 2008, **93**, 173305.
65 D. K. K. Liu and L. R. Faulkner, *J. Am. Chem. Soc.*, 1977, **99**, 4594–4599.
66 W. Yang, J. Zhao, G. Tang, X. Li and G. G. Gurzadyan, *J. Phys. Chem. Lett.*, 2019, **10**, 7767–7773.
67 T. Kobayashi, M. Yamashita, J. Du, J. Zhang and I. Iwakura, *Chem. Phys. Lett.*, 2013, **579**, 51–57.
68 J. Du, Z. Wang, W. Feng, K. Yoshino and T. Kobayashi, *Phys. Rev. B: Condens. Matter Mater. Phys.*, 2008, **77**, 19.
69 P. Muller, *Pure Appl. Chem.*, 1994, **66**, 1077–1184.
70 K. H. Wu, T. Y. Hsu, H. C. Shih, Y. J. Chen, C. W. Luo, T. M. Uen, J. Y. Lin, J. Y. Juang and T. Kobayashi, *J. Appl. Phys.*, 2009, **105**, 43901.
71 Z. Wu, H. Li, L. Yan, B. Liu and Q. Tian, *Superlattices Microstruct.*, 2013, **55**, 16–25.
72 M. Menšík, J. Pfleger and P. Toman, *Chem. Phys. Lett.*, 2017, **677**, 87–91.